JGP Journal of General Physiology

ARTICLE

Charybdotoxin binding to Shaker K+ channels is temperature sensitive in high external K+ but not in high external Na+

Nieves Navarro-Quezada[1,3], Francisca Salas-Sepulveda[2,4], Horacio Poblete[2], and David Naranjo[1]

Charybdotoxin (CTX), a peptide neurotoxin derived from the scorpion *Leiurus quinquestriatus*, binds to the external entrance of open voltage-gated K+ channels (VGKCs) with minimal conformational impact. By occluding the VGKC pore, CTX blocks passive K+ flow—a defining function of these membrane proteins. Due to its mechanistic simplicity and high signal-to-noise ratio, the CTX–VGKC interaction is an ideal system to investigate the molecular details of binding and unbinding. CTX bound to the Shaker VGKC exhibits thermal motion (wobbling) that permits access of external K+ to the channel pore. To test whether this wobbling is part of the reaction pathway during toxin–channel interaction, the energetic role of external K+ was examined in the association and dissociation kinetics. A high-affinity Shaker K427E-VGKC variant was expressed in *Xenopus* oocytes, and its activity was monitored via two-electrode voltage clamp between ∼10 and ∼30°C. Nanomolar applications of CTX to open and closed channels, in the presence of high external Na+ or high K+ concentrations, were used to measure blockade kinetics at different voltages and temperatures. In high K+, both the dissociation and association rates showed higher activation enthalpies, by ∼15 kJ/mol and ∼25 kJ/mol, respectively, compared with high Na+ conditions. However, the association rates under high Na+ and K+ were equal at ∼20°C, indicating a compensatory K+-induced activation entropy. We propose transient CTX-wobbling intermediates in both directions of the reaction pathway. Such a wobbling intermediate could enhance the diversity of productive collisions during association, increasing the efficacy of the scorpion venom.

Introduction

Protein–protein interactions are fundamental to numerous biological processes, ranging from enzymatic catalysis to signal transduction. The lifespan of these complexes can vary significantly, from milliseconds to years, depending on the binding energy involved. The association and dissociation pathways of protein complexes often involve the formation of high-energy transient intermediate states, collectively referred to as encounter complexes. These complexes are ruled by the activation energy barriers that determine the temperature sensitivity of reaction rates, as described by Arrhenius' principles (Dill and Bromberg, 2011). However, despite the valuable insights provided by MD simulations, the ephemeral nature of the encounter complex makes it difficult to capture molecular details through in vitro experiments. Here, we tested the temperature dependence of the association and dissociation kinetics of charybdotoxin (CTX) binding to voltage-gated potassium channels (VGKCs) in vitro to determine the Arrhenius parameters of the encounter/exit complex. This was assessed in the presence of K+, a permeant ion, and Na+, an impermeant one, to investigate the role of pore occupancy in shaping the energy landscape.

The CTX–VGKC system

CTX, a neurotoxic peptide derived from the venom of *Leiurus quinquestriatus*, blocks potassium channels and represents a mechanistically simple yet highly informative model for studying protein–protein interactions. This interaction produces robust electrophysiological signals that can be monitored at both macroscopic and single-molecule levels. The Chris Miller group showed first that CTX blocks potassium ion permeation by physically occluding the external pore entrance of large conductance calcium-activated potassium channel (BK), then they showed an identical mechanism for the blockade of VGKC (MacKinnon and Miller, 1988; Goldstein and Miller, 1993).

Structurally, VGKCs consist of homotetrameric α-subunits that form a central potassium-selective conduction pore surrounded by voltage-sensing domains (MacKinnon, 1991; Long et al., 2005). The selectivity filter, near the extracellular end of

[1]Instituto de Neurociencia, Universidad de Valparaíso, Valparaíso, Chile; [2]Centro de Bioinformática, Simulación y Modelado (CBSM), Facultad de Ingeniería, Universidad de Talca, Talca, Chile; [3]Centro Interdisciplinario de Neurociencia de Valparaíso, Valparaíso, Chile; [4]Doctorado en Ciencias mención Modelado de Sistemas Químicos y Biológicos, Universidad de Talca, Talca, Chile.

Correspondence to David Naranjo: david.naranjo@uv.cl.

the pore, interacts with CTX via key residues such as Lys27, which mimics potassium ions by binding to site S1 in the permeation selectivity filter (Ranganathan et al., 1996; Banerjee et al., 2013). Underscoring its mechanistic simplicity, crystallographic studies have revealed no discernible structural changes in the putative open conformation of VGKC upon CTX binding (Banerjee et al., 2013). In addition, pore-occluding scorpion toxin binding seems to be diffusion limited and electrostatically facilitated (Anderson et al., 1988; Miller, 1990; Escobar et al., 1993). These characteristics make CTX–VGKC an ideal model for exploring molecular pathways underlying protein complex association and dissociation.

CTX may wobble in its VGKC-binding site

An intriguing aspect of CTX–VGKC interaction is that the unbinding rate is sensitive to the K^+ concentration added at the external side, the same side from where the toxin acts. This outcome is incompatible with either a static toxin–channel interaction or total pore closure. We have known for some time that external potassium ions can access the selectivity filter while CTX remains bound. In fact, the location of the selectivity filter was deduced because permeant ions destabilize, from the external side, AgTx-2, a CTX isoform (Ranganathan et al., 1996). This destabilization occurs with a relative effectiveness that mirrors the ion permeation selectivity sequence (Moldenhauer et al., 2019). Since the structure of K^+ channels does not reveal any direct routes or fenestrations connecting the extracellular space to the selectivity filter, alternative pathways seem unlikely. A more intuitive explanation is that thermal motion induces dynamic behavior in the bound toxin, resulting in transient external accessibility that allows permeant ions to reach the selectivity filter. We refer to these dynamic partial detachments as "wobble." Supporting this hypothesis, the crystal structure of the CTX–VGKC complex in a Cs^+-rich solution shows the Lys27 amino group retracted into CTX, with site S1 occupied by a Cs^+ ion, suggesting alternative, possibly dynamic, binding arrangements (Banerjee et al., 2013). Given its ephemeral nature (see Discussion), wobbling may represent a transition state that contributes to the activation energy of CTX association and dissociation. To test this hypothesis, we examined how external ions, K^+, a permeant ion, and Na^+, an impermeant one, influence temperature dependence to assess the activation energies of CTX binding and unbinding to Shaker VGKC channels. We found (1) potassium-specific enthalpy and entropy components in both association and dissociation rate constants, and (2) the association rate in high external K^+ can be larger than that in high external Na^+. We propose that the dissociation and association pathways contain wobbling intermediates. In the association, it may increase the fraction of productive collisions between CTX and VGKC, being an evolutionary advantage in a neurotoxin.

Materials and methods

Heterologous expression of Shaker K channels

Our Shaker construct was derived from the Shaker H4 Δ(6–46) variant, inserted into the pBlueSK vector, and placed under the control of the T7 promoter (Agilent Technologies). The Shaker-K427E mutant was generated as previously described (Goldstein and Miller, 1992). Capped cRNAs were synthesized from a Not I-linearized template using the mMESSAGE mMACHINE T7 transcription kit (Ambion, Life Technologies), resuspended in 10 µl of water, and stored at −80°C. Female *Xenopus laevis* frogs were obtained from local suppliers and kept in captivity for several months. Typically, 0.03–0.3 ng of cRNA was injected into each *Xenopus* oocyte for heterologous expression, following protocols and guidelines described previously (Oliva et al., 2005; González-Pérez et al., 2008; Moscoso et al., 2012).

Electrophysiological recordings

Recordings from cRNA-injected oocytes were obtained ∼20–28 h after injection using the two-electrode voltage-clamp (TEVC) technique with a Warner OC-750C amplifier (Warner Instruments). The recording chamber measured 30 mm in length, 4 mm in width, and 3 mm in depth and was mounted in a Warner RC-24N/PM-1 heating/cooling module (Warner Instruments). Continuous perfusion was maintained with either *Hi-Na*$^+$ or *Hi-K*$^+$ recording solutions. The *Hi-Na*$^+$ solution contained (in mM): 96 NaCl, 2 KCl, 2 $CaCl_2$, 1 $MgCl_2$, and 10 HEPES (pH 7.4). For the *Hi-K*$^+$ solution, 96 mM NaCl was replaced with 96 mM KCl. CTX (Alomone Labs) was resuspended at 200 µM in Hi-Na^+ solution containing 25 µg/ml bovine serum albumin.

Electrodes were filled with 3 M KCl, 1 mM EGTA, and 5 mM HEPES (pH 7.0) and had resistances of ∼1 MΩ. The typical holding potential was −80 mV, and 500-ms voltage pulses (from −70 to +80 mV) were applied from a PC running either WinWCP software (University of Strathclyde, Glasgow, UK) or pClamp software (Molecular Devices), using either a PCI-MIO-16XE-10 card (National Instruments) or a Digidata 1440 (Molecular Devices), respectively.

Temperature was controlled using a TC2BIP controller (Cell MicroControls) interfaced with the Warner heating/cooling module. Recorded traces were exported into pClamp format (Molecular Devices) for signal analysis and curve fitting with Clampfit 10 (Molecular Devices). Data are presented as mean ± SD or, for fitted parameters of averaged data, as parameter ± SE of the parameter fit. Error propagation was performed as described by Diaz-Franulic et al. (2018). Data fits, within 95% confidence limit, were carried out using Origin 6.0 (OriginLab) with the Levenberg–Marquardt method. Statistical significance between curves was assessed using a modified χ^2 method that includes corrections for non-normality and sample size (Hristova and Wimley, 2023). Although some oocytes were used for measurements at different temperatures, most data can be assumed to be taken independently from separated cells.

Voltage-dependent relaxations to reveal CTX-binding kinetics

As observed with κ-conotoxin PVIIA (κ-PVIIA), a pore-blocking peptide toxin, the application of CTX to Shaker-K427E channels results in slow current relaxations upon channel opening. Voltage-dependent gating in the K427E variant is indistinguishable from that of the parent construct (Fig. 1 A; [Stocker and Miller, 1994]). These CTX-induced slow relaxations occur

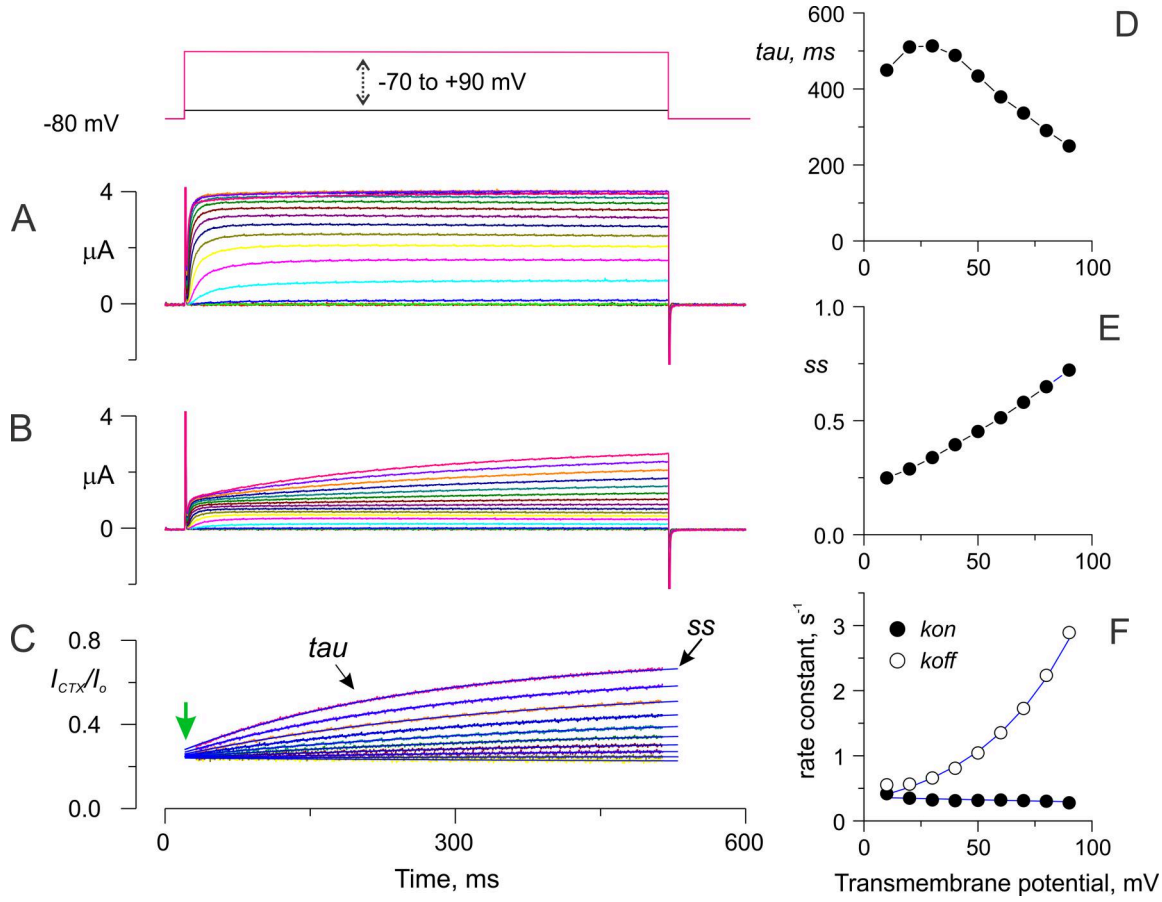

Figure 1. **Voltage dependency of the binding/unbinding kinetics. (A)**. Family of TEVC current traces, from an oocyte expressing Shaker K427E, elicited by 500-ms voltage pulses ranging from −70 to 90 mV (top panel). The oocyte was under continuous superfusion with the *Hi-Na*$^+$ recording solution (see Materials and methods). **(B)** Same as A, but plus 4 nM CTX. The trace coloring corresponds to the same voltage pulses in A. **(C)**. Point-by-point quotients between the trace with the toxin divided by it corresponding control trace in the interval 0–90 mV. The trace coloring is as in A and B. The blue line on top of each current-ratio trace are single-exponential fits with time constant, τ, and an equilibrium fractional inhibition, *ss*. **(D)** Plot of τ versus pulse voltage. **(E)** Plot of *ss* versus voltage. **(F)** The association and dissociation rates, k_{on} and k_{off}, for each voltage, calculated by solving the equation system 1, are plotted as a function of the voltage. The continuous lines were drawn with Eq. 4, where k_{V0} is the rate constant (k_{on} or k_{off}) at *Vm* = 0 mV and $z\delta$ is the effective valence of the voltage dependency. The solid lines were traced with Eq. 4 with parameters k_{off0} = 0.32 s^{-1}, $z\delta$ = +0.61 and k_{on0} = 0.093 nM^{-1}·s^{-1}, $z\delta$ = −0.06. See also Data S2 for underlying data.

because the same voltage pulse used to open the channels also destabilizes CTX binding in a voltage-dependent manner (García et al., 1999; Terlau et al., 1999; Moldenhauer et al., 2019; Naranjo and Díaz-Franulic, 2020).

The reaction Scheme 1 is the following:

$$\mathrm{Ch} + \mathrm{T} \underset{k_{off}}{\overset{k_{on}}{\rightleftharpoons}} \mathrm{Ch \cdot T} \qquad \text{Scheme 1.}$$

where *Ch* is an unblocked channel, *T* is the toxin, and *Ch•T* is a nonconductive channel–toxin complex. The association and dissociation rates, k_{on} and k_{off}, respectively, could be voltage dependent (see below). In response to a voltage pulse, the toxin binding relaxes exponentially to a new equilibrium, described by the relaxation time constant (τ), which is a function of the toxin concentration, as

$$\tau = \frac{1}{k_{on}[\mathrm{T}] + k_{off}} \qquad (1a)$$

Meanwhile, the fraction of unblocked channels in the new equilibrium (*ss*) is

$$ss = \frac{k_{off}}{k_{on}[\mathrm{T}] + k_{off}} \qquad (1b)$$

Together, Eqs. 1a and 1b provide a two-equation system with two unknowns, k_{on} and k_{off}, that can be solved from the experimental data. To analyze CTX-induced relaxations, we computed point-by-point ratio traces between linear leak–subtracted CTX-modified recordings (Fig. 1 B) and corresponding leak–subtracted control traces at the same voltage (Fig. 1 A). To minimize gating artifacts, we restricted analysis to voltage pulses above 20 mV and used a time window starting 15 ms after pulse onset and ending 5 ms before the pulse termination, ensuring that most channels remained open throughout (Moldenhauer et al., 2019). The resulting relaxations are plotted

in Fig. 1 C, using the same color scheme as Fig. 1, A and B. These point-by-point ratios traces were fit to a mono-exponential function (blue traces)

$$y = ss - (ss - ssc) \times \exp\left(-t/\tau\right), \quad (2)$$

where *ssc* represents the resting (closed state) fractional inhibition, extrapolated to the beginning of the pulse (green arrow in Fig. 1 C). From Eq. 2, for each voltage, we calculated

$$k_{off} = \frac{ss}{\tau}; \quad k_{on}[\mathrm{T}] = \frac{1}{\tau} - k_{off}.$$

To estimate the K_D from the point-by-point ratios, we used

$$K_D = [CTX] \times \left(\frac{1}{ss} - 1\right)^{-1} \quad (3)$$

We validated this method previously by showing that rapid application of κ-PVIIA to open channels and chronic exposure to the toxin yield identical relaxation kinetics and equilibrium inhibition, resulting in consistent rate constant estimates (García et al., 1999; Oliva et al., 2005). Fig. S1 shows a comparison of the k_{on} and k_{off} estimated from a kinetic analysis done at different CTX concentrations fitted with a variant of Eq. 1a

$$\frac{1}{\tau} = k_{on}[\mathrm{T}] + k_{off}.$$

This equation yields a straight line in a 1/τ versus [CTX] plot, where k_{on} is the slope and k_{off} is the intercept. The intercept, k_{off}, changes with the voltage pulse, while the slope remains nearly voltage independent, in good agreement with the results from the analysis using Eq. 2. We chose Eq. 2 over this methodology because with a single CTX concentration we can obtain k_{on} and k_{off} at different voltages. However, the single-concentration method becomes unreliable in *Hi-K*$^+$ conditions when the relaxation amplitude is low—e.g., when $ss \approx ssc$ (near +90 mV), or near the K^+ reversal potential (~0 mV; see Fig. 2). Therefore, for temperature dependence of the rate constants, we present temperature dependence data at +60 mV, where the signal-to-noise ratio was maximal.

The voltage dependence of rate constants was described by

$$k = k_{V0} \times \exp\left(\frac{z\delta FV}{RT}\right), \quad (4)$$

where k_{V0} is the rate constant (K_D, k_{on}, or k_{off}) at Vm = 0 mV. F, V, R, and T have their usual meanings; zδ is the effective valence of the voltage dependency. We described the effect of the temperature on the rate constants with

$$k = A \times \exp\left(\frac{-\Delta G^{\neq}}{RT}\right) = A \times \exp\left(\frac{-\Delta H^{\neq} + T\Delta S^{\neq}}{RT}\right)$$
$$= A \times \exp\left(\frac{\Delta S^{\neq}}{R}\right) \times \exp\left(\frac{-\Delta H^{\neq}}{RT}\right),$$
$$k = k_o \times \exp\left(\frac{-\Delta H^{\neq}}{RT}\right),$$

where $\Delta G^{\neq}$, $\Delta H^{\neq}$, and $\Delta S^{\neq}$ are the activation Gibbs energy, enthalpy, and entropy, respectively, and A is the Arrhenius pre-exponential factor. The rate constant k_o contains the frequency and entropic terms (Dill and Bromberg, 2011). Operationally, to estimate $\Delta H^{\neq}$ from the kinetic constants (in kJ/mol), we fitted the following expression to the rate constant versus T°C plots:

$$k = k_o \times \exp\left(\frac{-\Delta H^{\neq}}{0.0083(273 + T)}\right) \quad (5)$$

AI-use statement

The English in each paragraph (including this one) was individually checked using ChatGPT with the instruction "*check grammar*: 'Text paragraph…'." The content was then reviewed to ensure that no unintended changes in meaning were introduced.

Online supplemental material

Fig. S1 shows how the k_{on} and k_{off} were estimated using the variant of Eq. 1a. Data S1 contains the original data for the Figs. 1 and S1; Data S2 contains the original data for Fig. 2; Data S3 contains the original experimental traces used for Fig. 2; Data S4 contains a summary of experimental data in open channels for Figs. 3 and 5; Data S5 and Data S6 contain the data for Figs. 4 and 5.

Results

CTX-induced voltage-dependent relaxations in Shaker K channels

Shaker K channels expressed in *Xenopus* oocytes were recorded using the TEVC technique. CTX, at concentrations of 2–20 nM, was applied under continuous perfusion with either *Hi-K*$^+$ or *Hi-Na*$^+$ solution (see Materials and methods for details). The application of CTX to Shaker-K427E channels produces voltage-dependent relaxations in the hundreds-of-milliseconds range. Therefore, we chose to assess CTX blockade using 500-ms voltage pulses (compare Fig. 1, A and B).

Fig. 1, A and B, show two families of current traces obtained in *Hi-Na*$^+$ solution in response to voltage steps ranging from −70 to +90 mV (top panels), in the absence (Fig. 1 A) and presence (Fig. 1 B) of 4 nM CTX. CTX induces slowly increasing potassium currents, which correspond to relaxations from a high-affinity, closed-channel toxin-binding state to a lower-affinity, voltage-dependent binding regime in open channel (Scanlon et al., 1997; García et al., 1999; Terlau et al., 1999; Naranjo, 2002; Moldenhauer et al., 2019; Naranjo and Díaz-Franulic, 2020). The amplitude and kinetics of the relaxations increased with the voltage pulse amplitude, indicating that, in open channels, the toxin binding is destabilized by membrane depolarization. Fig. 1 C shows a family of point-by-point current ratios—CTX-modified traces divided by their corresponding control traces—for pulse voltages >0 mV (see Materials and methods). These ratios, plotted with the same color scheme as their parent traces, originate near a common value at the beginning of the pulse (green arrow), indicating the fractional inhibition in closed channels (*ssc*). As voltage increases, the amplitude and speed of the relaxations increase. These relaxation traces were fitted with Eq. 2 (blue traces), yielding estimates for *ssc*, the time constant (τ), and the steady-state inhibition at each voltage (*ss*; see Fig. 1, D and E).

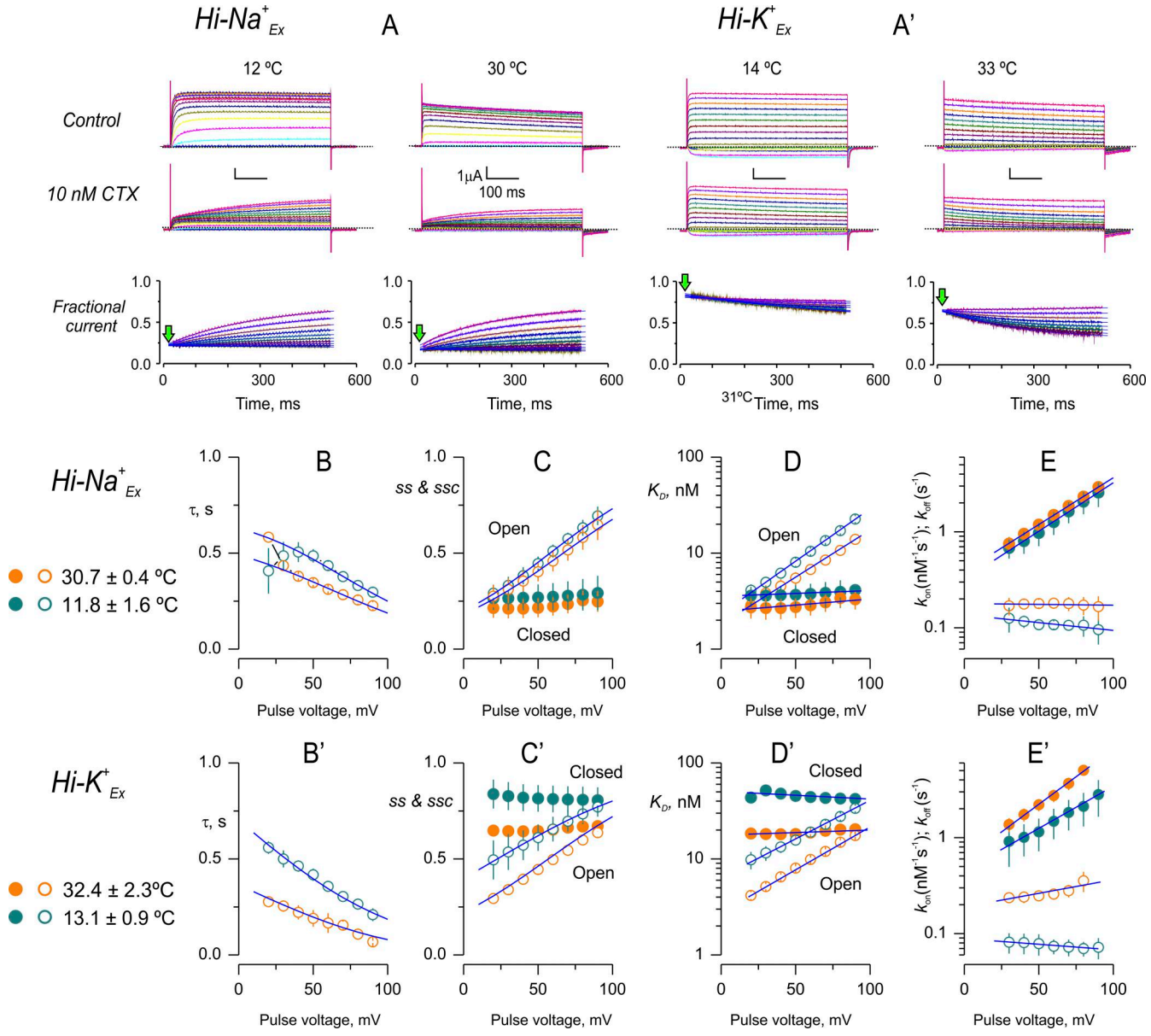

Figure 2. **Temperature dependence of CTX-induced relaxations in the presence of Hi-Na⁺ and Hi-K⁺ external solutions. (A and A′)** TEVC traces of measurements taken at temperatures separated by ~20°C in *Hi-Na*⁺ (A) and *Hi-K*⁺ (A′). Voltage pulse protocols and color coding are as in Fig. 1. Control: Traces in the absence of CTX; 10 nM CTX: Traces under continuous superfusion of recording solution plus 10 nM CTX; fractional current: Point-by-point quotients at different applied voltages at the temperatures shown on top of each panel. Upward relaxations indicate higher toxin affinity for closed channels in *Hi-Na*⁺ solutions, while downward relaxations in *Hi-K*⁺ indicate a higher affinity for the open channels. Eq. 2 fits are in blue. **(B and B′)** Comparison of the time constants, τ, in *Hi-Na*⁺ and *Hi-K*⁺, respectively. **(C and C′)** Comparison of the open channel asymptotic inhibition at different voltages (ss; open symbols) and closed state inhibition (ssc; green arrow; filled symbols). **(D and D′)** K_D calculated from Eq. 3 for open (open symbols) and closed channels (filled symbols). **(E and E′)** Rate constants as a function of voltage for the higher and lower temperature experiments. The continuous lines were drawn according to Eq. 4. The fitting values are the following: *Hi-Na*⁺; 11.8 ± 1.6°C: k_{off_o} = 0.33 ± 0.07 s^{-1}, zδ = 0.55 ± 0.07; k_{ono} = 0.14 ± 0.04 nM^{-1}s^{-1}, zδ = −0.11 ± −0.073; 30.7 ± 0.4°C: k_{off_o} = 0.37 ± 0.05 s^{-1}, zδ = 0.59 ± 0.02; k_{ono} = 0.17 ± 0.05 nM^{-1}s^{-1}, zδ = −0.067 ± 0.032; *Hi-K*⁺; 13.1 ± 0.9°C: k_{off_o} = 0.47 ± 0.21 s^{-1}, zδ = 0.49 ± 0.08; k_{ono} = 0.075 ± 0.014 nM^{-1}s^{-1}, zδ = −0.01 ± 0.05; 32.4 ± 2.3°C: k_{off_o} = 0.66 ± 0.1 s^{-1}, zδ = 0.64 ± 0.16; k_{ono} = 0.21 ± 0.02 nM^{-1}s^{-1}, zδ = 0.13 ± 0.06. All data points represent between three and six measurements. The parameter errors are the SD of the individual fits obtained with the Levenberg–Marquardt algorithm. See also Data S3 for underlying data.

Using Eq. 1a and 1b, we solved for the association and dissociation rates, k_{on} and k_{off}, for each voltage (Fig. 1 F). Consistent with a diffusion-limited association process, k_{on} values are high and only weakly voltage dependent (Miller, 1990; Goldstein and Miller, 1993). In contrast, k_{off} accounted for most of the voltage dependency of CTX binding, increasing approximately e-fold for every 40–50 mV of depolarization. The continuous lines in Fig. 1 F represent fits of Eq. 4 to the data. A summary of the fit parameters for CTX binding to Shaker-K427E in *Hi-Na*⁺ at 20°C is as follows: k_{off_o} = 0.22 ± 0.03 s^{-1}, zδ = +0.55 ± 0.05 (n = 10) and k_{ono} = 0.12 ± 0.01 nM^{-1}s^{-1}, zδ = −0.05 ± 0.06 (n = 10).

CTX binding to open channels is temperature dependent in *Hi-K*$^+$

To assess the contribution of potassium to the activation energy of CTX binding to Shaker channels, we compared kinetics in *Hi-K*$^+$ and *Hi-Na*$^+$ solutions at different temperatures. We measured the association and dissociation rates between ∼10°C and ∼30°C (see Materials and methods for details). Fig. 2 illustrates two representative temperature comparisons (Δt ≈ 20°C) in *Hi-Na*$^+$ (Fig. 2 A) and *Hi-K*$^+$ (Fig. 2 A′). The "Control" panels show current traces elicited by voltage pulses in the absence of toxin at 12°C and 30°C for *Hi-Na*$^+$ and at 14°C and 33°C for *Hi-K*$^+$. As previously reported, temperature increases both activation and inactivation kinetics (Meyer and Heinemann, 1997). The "10 nM CTX" panels display the corresponding currents in the presence of CTX (see Fig. 1), where inhibition in *Hi-Na*$^+$ appears stronger. The "Fractional current" panels show point-by-point current ratios in *Hi-Na*$^+$ and *Hi-K*$^+$; blue traces represent fits to Eq. 2. In this representation, CTX inhibition behaves very differently between solutions. First, in *Hi-K*$^+$, inhibition of closed channels is much weaker than in *Hi-Na*$^+$ (green arrows; *ssc* ∼0.60–0.85 versus ∼0.20–0.25, respectively). Second, the relaxation direction differs: in *Hi-K*$^+$, relaxations are downward rather than upward, indicating that, unlike in *Hi-Na*$^+$, CTX inhibition is stronger in open channels for most tested voltages. Thus, in *Hi-Na*$^+$, closed-channel inhibition resembles that of open channels at approximately +20 mV, while in *Hi-K*$^+$, it corresponds more closely to open-channel inhibition at approximately +90 mV. Third, relaxation kinetics remain voltage dependent in both conditions, becoming faster at more positive voltages. Fourth, in both *Hi-Na*$^+$ and *Hi-K*$^+$, toxin affinity for closed channels increases with temperature. In *Hi-Na*$^+$, *ssc* decreases from ∼0.25 at 12°C to ∼0.20 at 30°C, while in *Hi-K*$^+$, it drops from ∼0.85 at 14°C to ∼0.60 at 33°C. Fifth, the similarity in upward relaxations at 12°C and 30°C in *Hi-Na*$^+$ suggests that CTX inhibition of open channels is only modestly affected by temperature. In contrast, in *Hi-K*$^+$, temperature has a much more pronounced effect, as indicated by the larger amplitude of downward relaxations observed at 33°C. In summary, CTX displays higher affinity at elevated temperatures, and its binding kinetics to open channels in *Hi-K*$^+$ are more temperature sensitive than in *Hi-Na*$^+$.

The point-by-point current ratios shown in the Fractional current panels of Fig. 2, A and A′, were fit to Eq. 2 to obtain the parameters τ (the time constant), *ss* (the fractional inhibition at equilibrium), and *ssc* (the fractional inhibition of closed channels). Fig. 2, B–E and B′–E′, presents a comparative analysis based on several experiments similar to those in Fig. 2, A and A′, conducted at 11.8 ± 1.5°C (n = 5) and 30.7 ± 0.4°C (n = 3) in *Hi-Na*$^+$ and at 12.9 ± 0.9°C (n = 6) and 32.4 ± 2.3°C (n = 5) in *Hi-K*$^+$. Fig. 2, B and B′ show the temperature sensitivity of the average τ. A temperature increase resulted in a statistically significant ∼20% acceleration of relaxation in *Hi-Na*$^+$ (χ^2 = 58.1; P < 10^{-5}), while in *Hi-K*$^+$, the relaxation became approximately twofold faster (χ^2 = 200; P < 10^{-5}; Fig. 2 B′). Fig. 2, C and C′, displays the averages of *ss* and *ssc*, representing the equilibrium inhibition of open and closed channels (shown with open and filled symbols, respectively). A comparison of Fig. 2, C and C′, reveals that in both conditions, binding to closed and open channels increases with temperature. However, the increase is significantly more pronounced in *Hi-K*$^+$ (χ^2 = 106; P < 10^{-5} for *ss* and χ^2 = 102; P < 10^{-5} for *ssc*), whereas in *Hi-Na*$^+$, the changes in *ss* and *ssc* are not statistically significant (χ^2 = 7.28; P = 0.507 for *ss* and χ^2 = 8.41; P = 0.395 for *ssc*).

In terms of binding affinity, these differences translated into K_D calculated using Eq. 4 (Fig. 2, D and D′; open and filled symbols depict open and closed channels, respectively). For both experimental conditions, the effect of the temperature on K_D in open and closed channels is similar but more pronounced in *Hi-K*$^+$. After fitting Eq. 4 to K_D data (solid lines in Fig. 2, D and D′), we observed the following: in *Hi-Na*$^+$, the K_D for open channels decreased from K_{D0} = 2.32 ± 0.058 nM with zδ = 0.62 ± 0.01 to K_{D0} = 1.78 ± 0.07 nM with zδ = 0.59 ± 0.01 (values are fit parameter ± SE of the fit). Meanwhile, in *Hi-K*$^+$, the K_D for open channels decreased from K_{D0} = 6.33 ± 0.53 nM with zδ = 0.45 ± 0.03 to K_{D0} = 2.2 ± 0.5 nM with zδ = 0.57 ± 0.08. Similar changes were observed in closed channels: in *Hi-Na*$^+$, the K_D decreased from K_D = 3.57 ± 0.12 nM to K_D = 2.51 ± 0.13 nM. Meanwhile, in *Hi-K*$^+$, the K_D decreased from K_D = 48.03 ± 0.85 nM to K_D = 17.91 ± 0.95 nM. These results indicate that, under both ionic conditions, increasing the temperature enhances the binding affinity of CTX.

Fig. 2, E and E′, shows a comparison of the resulting kinetic rate constants in *Hi-Na*$^+$ and *Hi-K*$^+$ solutions, respectively. In both experimental conditions, k_{on} is more temperature sensitive. Notably, k_{on} in *Hi-K*$^+$ (orange open circles in Fig. 2 E′) seems to be the most temperature-sensitive rate constant, showing a three- to fourfold increase, compared with less than twofold increase in *Hi-Na*$^+$. The dissociation rate in *Hi-K*$^+$ also increased significantly at all voltages tested, whereas in *Hi-Na*$^+$, the differences between the two temperatures were not statistically significant (χ^2 = 10.6; P value = 0.16). In summary, only k_{off} in *Hi-Na*$^+$ appears temperature insensitive.

Fig. 3 summarizes the temperature dependence of CTX binding to open Shaker channels in *Hi-Na*$^+$ and *Hi-K*$^+$. Fig. 3 A plots the K_D at zero voltage, K_{Do}, obtained from fits of Eq. 4 to data as shown in Fig. 2, D and D′. K_{Do} is reduced to a half in *Hi-K*$^+$, while the changes in *Hi-Na*$^+$ remain within the range of data dispersion. Such a temperature dependence in *Hi-K*$^+$ points to an additional ΔΔG = ∼24 kJ/mol when K^+ replaces external Na^+, corresponding to an ∼20,000-fold difference in affinity at room temperature (20°C). The effective valence of the voltage dependency, zδ, the other parameter of Eq. 4, shows negligible variation in *Hi-Na*$^+$. In contrast, in *Hi-K*$^+$, zδ increases by ∼0.2e with temperature (Fig. 3 B). Since this additional voltage dependence could be artifactual (see Materials and methods), we used the average association and dissociation rates measured at +60 mV, where the signal-to-noise ratio is highest, to calculate enthalpies (50–70 mV; Fig. 3, C–D). Fig. 3 C shows that at ∼13°C, the dissociation rates constants, k_{off}, are similar in both ionic conditions. However, at ∼30°C, k_{off} in *Hi-K*$^+$ is approximately twofold larger than in *Hi-Na*$^+$. In this later ionic condition, k_{off} is not temperature sensitive. In contrast, the association rate shows more dramatic temperature dependence (Fig. 3 D): it increases three- to fourfold in *Hi-K*$^+$, compared with only ∼50% in *Hi-Na*$^+$. Interestingly, this greater temperature sensitivity causes k_{on} in *Hi-K*$^+$ to surpass that in *Hi-Na*$^+$ at temperatures

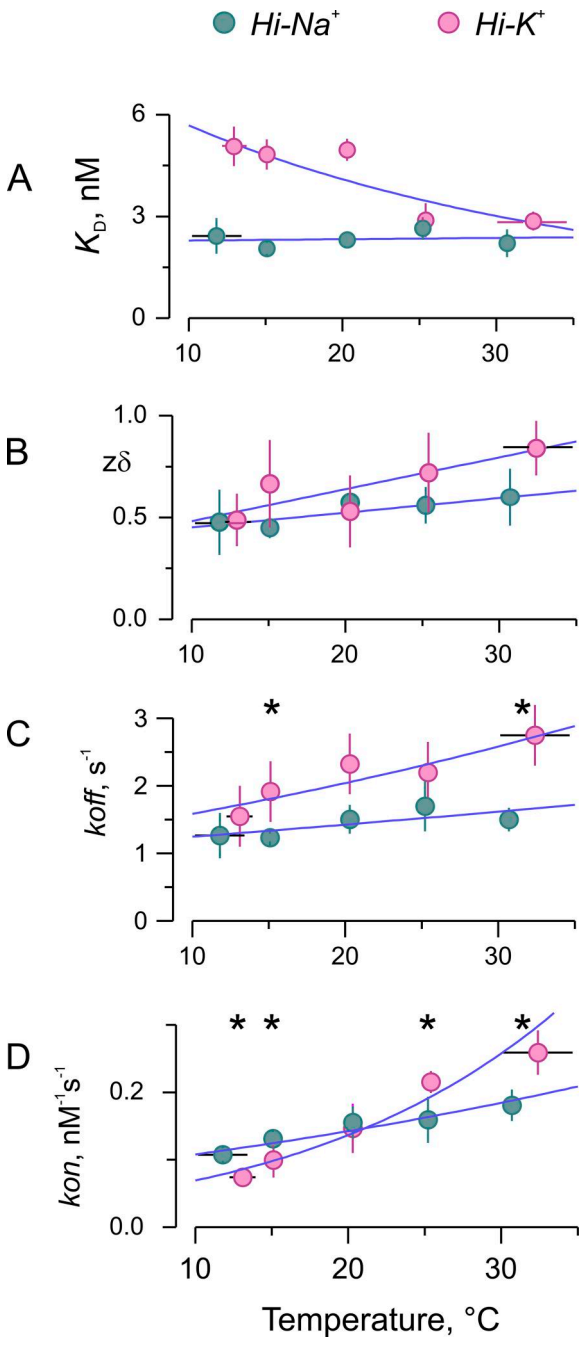

Figure 3. **Temperature dependency of the rate and equilibrium constants to open channels in Hi-Na⁺ and in Hi-K⁺ (cyan and pink symbols, respectively). (A)** The K_D at 0 mV. K_D were calculated from Eq. 3 with the determination of ss at different voltages and fit to Eq. 4 (Fig. 2, D and D′). The continuous lines are drawn assuming ΔG° = 22.6 kJ/mol for *Hi-K*⁺ and −1.2 kJ/mol for *Hi-Na*⁺. Vertical error bars are the standard error of the fit. Horizontal error bars are SD. **(B)** Effective valence of the voltage dependency (zδ) from the above fits to Eq. 4. The solid lines do not have any physical meaning. Vertical error bars are the SE of the fit. **(C)** Dissociation rate constant measured at +60 mV (see Fig. 2, E and E′). The solid lines were drawn from Eq. 5 with $\Delta H^{\neq}$ = = 9.3 ± 5.9 kJ/mol and 17.2 ± 3.8 kJ/mol for *Hi-Na*⁺ and Hi-*K*⁺, respectively (standard error of the fit). Horizontal error bars are SD. **(D)** Association rate constant measured at +60 mV (see Fig. 2, E and E′). The solid lines were drawn from Eq. 5 with $\Delta H^{\neq}$ = = 19.1 ± 5.4 kJ/mol and 46.9 ± 7.1 kJ/mol for *Hi-Na*⁺ and *Hi-K*⁺, respectively. In C and D, data are mean ± SD; asterisks indicate statistical differences between data obtained at similar temperatures (P value <0.05). See also Data S4 for a summary of experimental data in open channels.

above ~20°C. While surprising, similar observations have been reported for Shaker: the CTX-R25Q variant showed a twofold higher association rate in high external K⁺; and low ionic strength experiments revealed an approximately fourfold higher association rate in K⁺ solutions compared with Na⁺ solutions (Goldstein and Miller, 1993; Moldenhauer et al., 2019). Binding to BK channels has also been observed to occur about twice as fast in K⁺ compared with Na⁺ solutions (Anderson et al., 1988). In summary, we found that CTX binding to open Shaker K channels in *Hi-K*⁺ exhibits greater temperature sensitivity in both association and dissociation rate constants than in *Hi-Na*⁺. This enhanced sensitivity suggests the presence of K⁺-dependent enthalpic components in both the association and dissociation pathways of CTX binding.

CTX binding to closed channels is also temperature dependent in *Hi-K*⁺

CTX-binding equilibrium to the closed BK and VGKC is voltage independent (Anderson et al., 1988; Goldstein and Miller, 1993; Moldenhauer et al., 2019). This property allows for a clear separation of voltage dependence from potassium dependence. To evaluate CTX-binding kinetics to closed channels, we used a two-pulse protocol previously developed for κ-PVIIA (Terlau et al., 1999; Naranjo and Díaz-Franulic, 2020). In this protocol, a first conditioning voltage pulse significantly alters the CTX-binding equilibrium (Fig. 4, A and B, top). Then, after a variable inter-pulse interval at the holding voltage, a second (test) pulse is applied to assess the time course of the return to the closed-channel CTX-binding equilibrium. Fig. 4, A and B, shows 10 current traces obtained using this two-pulse protocol in *Hi-Na*⁺ (Fig. 4 A) and *Hi-K*⁺ (Fig. 4 B) at 25°C. The blue dots in Fig. 4, A and B, represents isochronal current amplitudes measured 5–10 ms after the onset of the test pulse. A single-exponential function was fitted to the data (solid lines) to determine the time constant (τ) for closed-channel binding. Fig. 4 C shows that the time constants in *Hi-K*⁺ exhibit greater temperature sensitivity over the tested range (~15 to ~32°C; green and pink symbols represent *Hi-Na*⁺ and *Hi-K*⁺, respectively). For the closed-channel equilibrium blockade (*ssc*) at various temperatures (Fig. 4 D), we used the average of the convergence points from the point-by-point ratios shown in Fig. 2, C and C′ (see Naranjo and Díaz-Franuli [2020]). Applying the equation system 1 to these data allowed us to calculate k_{on} and k_{off} for closed channels at different temperatures (open and filled symbols, respectively) in *Hi-Na*⁺ and *Hi-K*⁺ (Fig. 4 E). As with open channels, both association and dissociation rates in *Hi-K*⁺ showed greater temperature sensitivity than in *Hi-Na*⁺. Interestingly, at lower temperatures, the association rate in *Hi-Na*⁺ is threefold higher than in *Hi-K*⁺; however, near 35°C, as observed in open channels, the association rate in *Hi-K*⁺ surpassed that in *Hi-Na*⁺. Thus, the temperature-dependent behavior of CTX binding is similar in both open and closed channel conformations.

The solid lines in Fig. 3, C and D; and Fig. 4 E correspond to fits of Eq. 5 to the temperature dependence of the rate constants. Fig. 5 summarizes the estimated activation enthalpies ($\Delta H^{\neq}$) derived from the temperature dependence of the rate constants

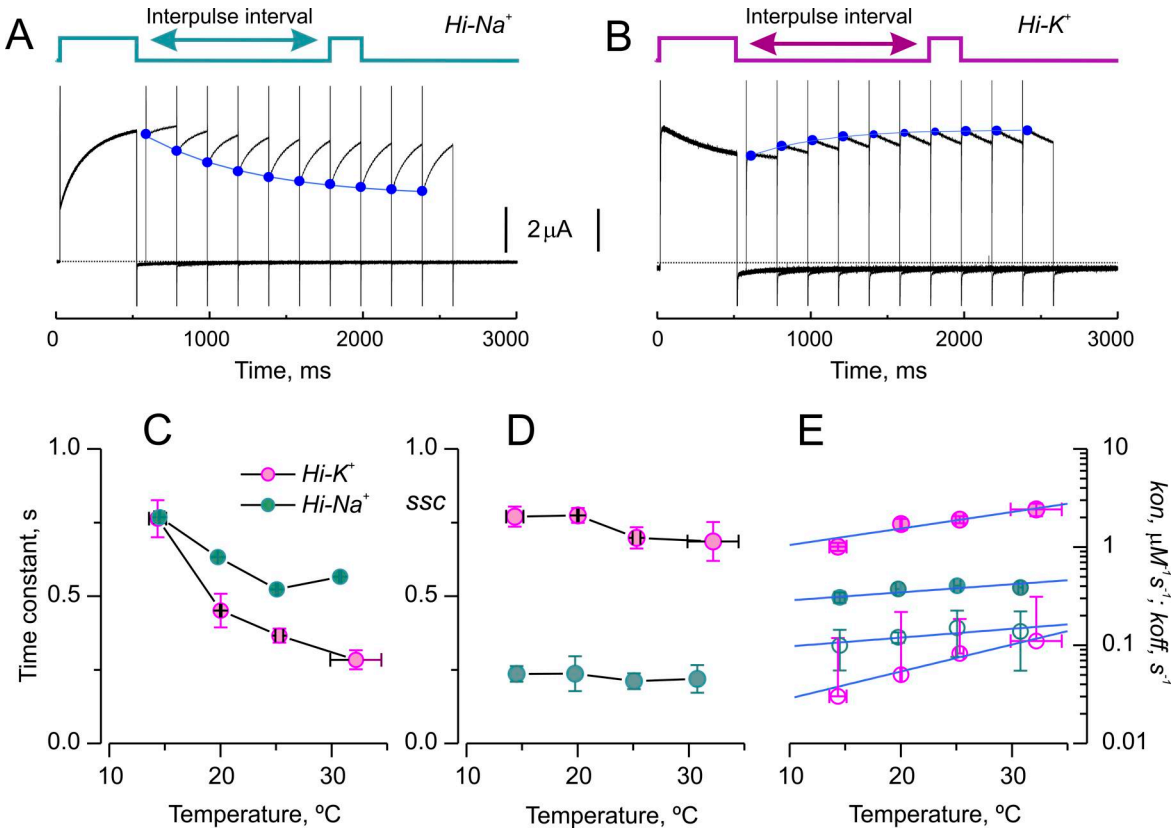

Figure 4. **CTX binding to closed channels. (A and B)**, Two-pulse protocol to measure CTX-blockade kinetics to resting channels in *Hi-Na*$^+$ (A) and *Hi-K*$^+$ (B) solutions (for A and B, T° ~25°C). A 500-ms prepulse to +50 mV was followed by a second 200-ms test pulse to +50 mV after a variable interpulse interval at −90 mV (top inset). The kinetics of reinhibition at resting produced by 10 nM CTX in the bath was estimated by measuring the average currents in a 5-ms interval between 5 and 10 ms into the test pulse current. These inhibition values are plotted as filled blue circles along each set of traces and fitted to a single exponential to estimate the time constant of toxin rebinding. **(C)** Time constants in *Hi-K*$^+$ are more T° sensitive in the 15–33°C interval. **(D)** Steady-state resting inhibition, measured at the point of convergence of the traces as shown in Figs. 1 and 2 (green arrows). **(E)** Summary of temperature dependence of the association (open symbols) and dissociation rate constants (filled symbols) in *Hi-Na*$^+$ and *Hi-K*$^+$ obtained from equation system #1 for several temperatures. The solid lines were traced from Eq. 5 with $\Delta H^{\neq}$ = 17.3 ± 6.7 kJ/mol and $\Delta H^{\neq}$ = 11.3 ± 6.2 kJ/mol for k_{on} and k_{off}, respectively, in *Hi-Na*$^+$ solutions, and $\Delta H^{\neq}$ = 45.7 ± 8.7 kJ/mol and $\Delta H^{\neq}$ = 27.1 ± 6.7 kJ/mol for k_{on} and k_{off}, respectively, in *Hi-K*$^+$ solutions (see main text). See also Datas S5 and S6 for underlying data.

for both open and closed channels in *Hi-Na*$^+$ and *Hi-K*$^+$ solutions (in cyan and pink bars, association [open bars] and dissociation [filled bars], respectively). In both channel conformations, k_{on} in *Hi-K*$^+$ shows the largest contribution to temperature dependence, with $\Delta H^{\neq} \approx 45$ kJ/mol. In contrast, $\Delta H^{\neq}$ for k_{off} ranges between 17 and 27 kJ/mol and is consistently higher in *Hi-K*$^+$ than in *Hi-Na*$^+$ (filled bars). Despite the use of different experimental methodologies used to estimate k_{on} and k_{off} (single-pulse for open channels versus multiple-pulse in closed channels), the consistency of the results supports a specific effect of K$^+$ ions on the $\Delta H^{\neq}$ of association and dissociation in open and closed channels. Interestingly, although the activation enthalpy of k_{off} is ~24 kJ/mol larger in *Hi-K*$^+$ than in *Hi-Na*$^+$, the association rates are nearly identical at 20°C, suggesting the presence of a K$^+$-specific activation entropy ($\Delta S^{\neq}$) of about 82 J/mol•K, which compensates for the potassium-dependent increase in enthalpy.

Discussion

The most prominent and surprising finding of this study is that, in high external K$^+$ solutions, the activation enthalpy of CTX association and dissociation from the Shaker K channel is greater than in high external Na$^+$ solutions (Fig. 5). Considering that k_{on} is expected to be diffusion limited in both *Hi-K*$^+$ or in *Hi-Na*$^+$ solutions, this K$^+$-dependent increase in activation enthalpy is unexpectedly high (Escobar et al., 1993). Moreover, at temperatures above 20°C, the association rate in high external K$^+$ surpasses that observed in high external Na$^+$ (Fig. 3 C and Fig. 4 E)—a counterintuitive result, as potassium competes with CTX for binding to the pore (see, for example, Ranganathan et al., 1996; Moldenhauer et al., 2019). In the following paragraphs, we discuss why these two findings, along with the external K$^+$ sensitivity of the dissociation rate, represent unexpected results.

Wobbling

The toxin dissociation rate in *Hi-K*$^+$ is approximately twice as high as in *Hi-Na*$^+$, as shown in Fig. 3 C. This result is consistent with earlier electrophysiological findings indicating that high external K$^+$ reduces toxin affinity (Ranganathan et al., 1996). Additional support for this idea comes from two observations: (1) the CTX K_D follows the same selectivity sequence as permeation and (2) the *external* ion selectivity of the dissociation rate

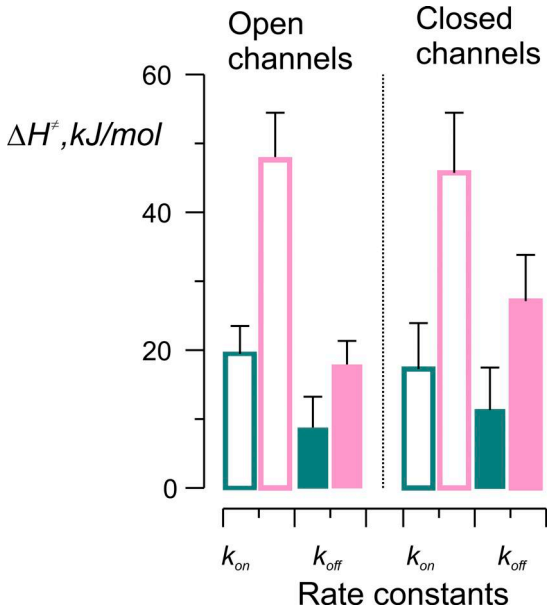

Figure 5. **Activation enthalpy of CTX binding to open (left) and closed channels (right).** The values of $\Delta H^{\neq}$ were estimates from Eq. 5. Cyan and pink bars denote measurements in *Hi-Na*$^+$ and *Hi-K*$^+$, respectively, while open and filled bars correspond to k_{on} and k_{off}, respectively. Error bars are the SE of the fit. See also Data S4 for a summary of experimental data in open channels and Datas S5 and S6 for underlying data.

enhancement in Shaker mirrors the *internal* ion selectivity observed in BK channels (Anderson et al., 1988; Moldenhauer et al., 2019). Access to the selectivity filter during CTX binding could be explained in two ways: either CTX transiently unbinds from the pore, or—similar to the μ-conotoxin blockade of the SCN4A Na^+ channel—the toxin only partially occludes the pore (French et al., 1996). Gating current measurements of Shaker K channels blocked with AgTx-2 offer insight into this distinction. Aggarwal and MacKinnon (1996) using TEVC in *Xenopus* oocytes, observed that ∼10^{10} toxin-blocked Shaker channels produced <1 μA of ionic current at +50 mV. From this, we estimate that the residual unitary current of blocked channels must be < 0.1 fA—that is, <0.01% of the current from unblocked channels. If the toxin only partially blocks the pore, it would leave a clearance with an effective radius of about 10 fm, assuming that the radius of capture for K^+ ions in Shaker channels is ∼0.8 Å (Díaz-Franulic et al., 2015; Moldenhauer et al., 2016). This dimension is implausibly small at the molecular scale unless we consider that the interaction between CTX and the channel is dynamic. Thus, this external accessibility likely results from transient fluctuations of the bound toxin caused by thermal motion. Consequently, the idea that the toxin briefly unbinds, allowing the pore to be accessible for <0.01% of the time, is both simpler and more intuitive. Furthermore, since the pore is formed by the close apposition of all four subunits, a partial occlusion model cannot easily account for the observation that AgTx-2 simultaneously contacts all four residue-449 positions around the Shaker pore (Gross and MacKinnon, 1996). Therefore, to permit access of external ions to the selectivity filter, one or more of these 449-residue contacts must intermittently separate from the toxin. This implies that the bound CTX undergoes dynamic movement, trembling, or wobbling, which could be facilitated by potassium ions occupying the S1 site in the selectivity filter.

A structural interpretation of the K^+-dependent enthalpy and the occupation of the selectivity filter

CTX binds to the open VGKCs with a simple 1:1 lock and key mechanism (Goldstein and Miller, 1993; Banerjee et al., 2013). The structure of the CTX/Kv1.2 channel complex reveals a tightly complementary interaction surface, with only minor structural differences compared with the toxin-free, presumably open, Kv channel structure (PDB ID 4JTA and PDB ID 2R9R for the complex and channel alone, respectively [Banerjee et al., 2013]). In the toxin–channel complex, S1, the outermost K^+-binding site in the selectivity filter, lacks K^+ electron density. Instead, the amino group of Lys27 in CTX occupies this site, effectively mimicking a K^+ ion (Banerjee et al., 2013). Supporting this interpretation, a cryo-EM structure of the sea anemone toxin *ShK* bound to the Kv1.3 channel also shows a lysine amino group mimicking a K^+ ion at S1 (Selvakumar et al., 2022).

These structural features strongly support the most prominent functional effect of CTX binding: the physical occlusion of the pore, which blocks ionic current (Figs. 1 and 2). As shown in Figs. 1 and 2, increasing the internal voltage accelerates the dissociation rate, k_{off}, with an effective electrical valence of $z\delta$ ∼0.5 e_o (see Fig. 3 B). This voltage effect likely reflects the outward movement of K^+ ions in the selectivity filter, destabilizing CTX (MacKinnon and Miller, 1988). While this model, originally proposed for BK channels, explains part of the Shaker K channel behavior, it does not fully account for it. In Shaker channels, removing internal K^+ reduces the effective valence of the voltage sensitivity by half, rather than eliminating it, as observed in BK channels. This suggests a weaker coupling between pore occupancy and CTX voltage sensitivity (Goldstein and Miller, 1993).

Compared with experiments in *Hi-Na*$^+$, potassium contributes ∼25 kJ/mol to the activation enthalpy of association and 10–20 kJ/mol to the dissociation enthalpy in *Hi-K*$^+$ for both open and closed channels. These values are in line with prior estimates of the 20–25 kJ/mol energy difference in Na^+ versus K^+ permeation, derived from energy calculations and electrophysiological evaluations of KcsA, a structurally well-characterized K^+ channel (Aqvist and Luzhkov, 2000; Bernèche and Roux, 2001; LeMasurier et al., 2001). This figure is consistent with the selectivity ratio P_{Na+}/P_{K+} < 0.01 estimated from reversal potential measurements in Shaker channels (Heginbotham and MacKinnon, 1993; Díaz-Franulic et al., 2015; Naranjo et al., 2016) and with an affinity ratio of ∼0.001 estimated for the outer binding site, likely S1, of the BK channels in the presence of Ba^{2+} in the pore (Neyton and Miller, 1988). Thus, the additional activation enthalpy observed in the toxin rate constants may reflect the differing occupancy of the selectivity filter by Na^+ versus K^+ ions. In this context, it is reasonable to expect a K^+-specific enthalpic penalty for CTX binding, since in *Hi-K*$^+$, the S1 site would be occupied more frequently by K^+, thereby hindering binding of the Lys27 side chain (Ranganathan et al., 1996; Banerjee et al., 2013; Moldenhauer et al., 2019).

The large enthalpy of k_{on} is not consistent with a purely diffusion-controlled rate

Miller (1990) found that viscosity reduces both the association and dissociation rates of CTX binding to BK channels by similar extents, suggesting a diffusion-controlled reaction. Given the large k_{on} for the CTX–Shaker system (~10^8 $M^{-1}s^{-1}$; Fig. 3 E), it is tempting to propose a similar diffusion-limited mechanism. If CTX were modeled as a sphere colliding with a hemispherical sink at the channel's external mouth, the diffusion-controlled rate constant, k, would follow the Smoluchowski limit

$$k = 2\pi r_c DC,$$

which is an intuitive expression in which D is the diffusion coefficient, C is the molar concentration of the solute, and r_C is the effective capture radius, the difference between the sphere radius and the receptor radius (Miller, 1990; Dill and Bromberg, 2011). Just by assuming $D = 10^{-6}$ cm^2s^{-1} for CTX and $r_C = 2.5$ Å, we can make k_{on} reach ~10^8 $M^{-1}s^{-1}$, as in Fig. 3 results. However, the magnitude of k_{on} alone can be misleading when interpreting CTX binding to Shaker as a diffusion-limited process. For instance, under low ionic strength (~0.02 M) conditions with predominantly K^+ present, CTX binds Shaker with a k_{on} ~35 times higher (~3.5×10^9 $M^{-1}s^{-1}$) (Moldenhauer et al., 2019). This extremely high rate would require unrealistic assumptions to fit the Smoluchowski limit: (1) A receptor acting as a hemispheric sink with a ~100 Å radius; (2) a 35-fold increase in local toxin concentration; or (3) a 35-fold increase in the diffusion coefficient. First, a ~100-Å sink is unrealistically large, much greater than the actual dimensions of Kv channels. Second, a 35-fold increase in local CTX concentration would imply the presence of two dense layers of toxin molecules (~20-Å diameter) adsorbed to the channel surface. Third, an effective 35-fold increase in the diffusion coefficient would require CTX to behave like a particle of subatomic size. Unless long-range electrostatic interactions are invoked, the diffusion-limited hypothesis fails to explain such large association rates. Getting closer to the diffusion limit may be possible if a large fraction of collisions occur in the correct orientation, aided by pre-binding electrostatic steering (Escobar et al., 1993). Alternatively, an important percentage of the collisions would be effective if electrostatic steering allowed postcollision complexes rearrangement to find the fully bound conformation.

CTX is a positively charged peptide (+5), then its association rate can be shaped by the electrostatic attraction to the negatively charged mouth of the channel. This kind of attraction occurs through an electrostatically transparent environment that is screened by a fog of dissolved ions (or ionic strength). The ionic strength interferes with the association rate according to the Brønsted–Bjerrum equation (Castaneda-Agullo et al., 1961). In fact, in κ-PVIIA (charge +4), the electrostatically assisted rate decreases exponentially with the square root of the ionic strength if a charge of −2.5 is assigned to the Shaker vestibule (Naranjo and Díaz-Franulic, 2020). While this model can approximate the magnitude of the association rate enhancement, it oversimplifies the interaction by treating it as the collision of two point charges. In reality, the CTX molecule is over 8 Å in diameter, comparable with the Debye length at 0.15-M ionic strength, and probably must align precisely with the receptor for binding to be productive.

Thus, a very large association rate likely arises from a combination of factors, all with weak temperature dependence, such as local concentration increases, electrostatic attraction, and steering into the correct orientation for productive binding (Miller, 1990; Volkov et al., 2006; Harel et al., 2009; Schreiber et al., 2009). Therefore, the high activation enthalpy must originate from a postbinding step.

K^+ uncovers an encounter complex

The CTX-binding process may involve a two-step mechanism in which a relatively long-lived encounter (or intermediate) complex is formed (Escobar et al., 1993; Schreiber et al., 2009). Before reaching the final Shaker–CTX-blocked conformation, the toxin likely diffuses into the channel vestibule, where short- and long-range contact rearrangements occur before CTX finally "clicks" into the S1 site. For dissociation, the toxin must retrace this path, breaking weak and strong bonds, disengaging contact surfaces, and detaching from the receptor. We can represent this with the following reaction in Scheme 2:

$$Ch + Tx \underset{k_{-1}}{\overset{k_1}{\rightleftharpoons}} Ch * Tx \underset{k_{-2}}{\overset{k_2}{\rightleftharpoons}} Ch \cdot Tx \qquad \text{Scheme 2.}$$

In this Scheme 2, the association between the channel (*Ch*) and the toxin (*Tx*) forms an intermediate complex (or encounter complex), *Ch*Tx*, with k_1 and k_{-1} being diffusion limited. The second step corresponds to the formation (k_2) and dissociation (k_{-2}) of the fully bound and long-lived complex, *Ch•Tx*. This latter step may be observed as a chemical reaction involving configurational rearrangements, transient interactions, interfacial de-wetting, and electrostatic pairing and complementarity (Schreiber et al., 2009)

$$k_a = \frac{k_1 k_2}{k_{-1} + k_2} \tag{6}$$

Meanwhile, the dissociation rate is

$$k_{-a} = \frac{k_{-1} k_{-2}}{k_{-1} + k_2} \tag{7}$$

If $k_{-1} >> k_2$

$$k_a \sim \frac{k_1 k_2}{k_{-1}} \quad \text{and} \quad k_{-a} \sim k_{-2}.$$

If k_2 and k_{-2} are temperature-dependent, both k_a and k_{-a} would contribute significantly to the enthalpy of activation. We assume that Scheme 2 holds under both *Hi-K*$^+$ and *Hi-Na*$^+$ experimental conditions. However, the high enthalpy observed in *Hi-K*$^+$ (Fig. 5) likely results from a K^+-dependent reduction of k_2 and possibly an acceleration of k_{-2}. Interestingly, if the association rate is limited by the number of effective collisions, the rate remains diffusion controlled.

The interaction interface between the toxin and the Shaker channel is large (~50–100 Å^2), with many residues on both surfaces contributing sticky contacts. We propose that the formation of the *Ch*Tx* intermediate is facilitated by complementary electrostatics,

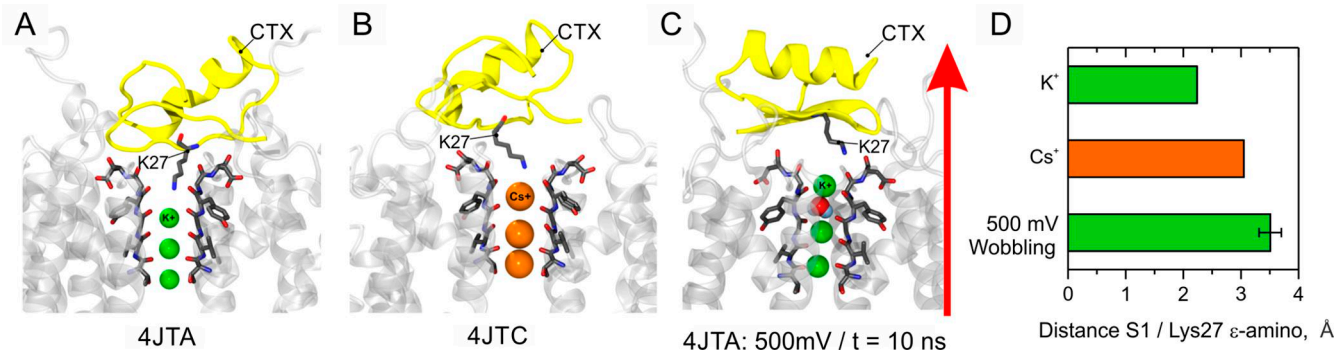

Figure 6. **Interaction of CTX Lys27 side chain with the Kv1.2/2.1 K^+ channel selectivity filter. (A)** Structure in K^+ salt (PDB ID 4JTA) shows the S1 site in the selectivity filter occupied by the Lys27 ε-amino group. **(B)** Structure in Cs^+ salt (PDB ID 4JTC) shows the S1 site occupied by a Cs^+ ion instead of the Lys27 ε-amino group. **(C)** Representative conformation from an all-atom MD simulation of the 4JTA Kv channel structure, in which an outward transmembrane electric field of 500 mV was applied after equilibration. This frame was taken ∼10 ns after the application of the electric field to the protein–membrane complex. The red arrow indicates the direction of the electric field (only two subunits of the tetramer are shown). **(D)** Distance between the Lys27 ε-amino group and the center of mass of the four Kv1.2-Y373 carbonyl oxygens in the K^+ and Cs^+ structures. These data are compared with the average over a 10-ns time window, beginning 5 ns after the application of a 500-mV transmembrane electric field in an MD simulation ("500 mV Wobbling"). The error bar for the MD data represents the SD of the mean distance. 4JTA and 4JTC are creation by Banerjee et al. (2013). MD data were extracted from the CTX–Kv1.2 protein complex model used by Moldenhauer et al. (2019).

which play a key role in attracting and steering the toxin into a favorable orientation. As a result, the complex likely explores several contact geometries before achieving full binding, with the ε-amino group of Lys27 ultimately clicking into the S1 site. This scenario implies that a large fraction of protein–protein encounters are productive, provided that electrostatically aided collisions are followed by a stochastic search for the correct configuration. In fact, this mechanism appears to be general. Other well-studied protein–protein systems, such as barnase–barstar, cytochrome c and its oxidase, and trypsin with its inhibitor BPTI, also exhibit steering and reaccommodation of binding peptides, allowing a large fraction of collisions to be effective (Schreiber and Fersht, 1995; Frisch et al., 2001; Volkov et al., 2006; Kahler et al., 2020).

Despite the large K^+-dependent activation enthalpy (∼25 kJ/mol), both kinetic rate constants (k_a and k_{-a}) are similar in *Hi-K*$^+$ and *Hi-Na*$^+$ at 20°C (Fig. 3 C and Fig. 4 E). If the difference between Na^+ and K^+ binding were solely due to the enthalpy of the transition state, CTX binding in high Na^+ solutions would be predicted to be ∼20,000-fold faster. However, the observed similarity in association rates implies that the excess K^+-dependent $\Delta H^{\neq}$ is offset by a compensating K^+-dependent $\Delta S^{\neq}$ of ∼82 J/mol·K. A simplistic interpretation of these thermodynamic parameters is that, despite the enthalpic penalty imposed by K^+, the *Ch*Tx* intermediate exhibits a large gain in conformational entropy, suggesting ∼20,000 more accessible pathways to reach the fully bound state at 20°C.

In addition to the large K^+-specific $\Delta H^{\neq}$, we identified a notable inconsistency with the classical model of diffusion-controlled CTX binding to Shaker. At temperatures above 20°C, and despite the competitive relationship between K^+ and CTX, the toxin's association rate in *Hi-K*$^+$ can surpass that in *Hi-Na*$^+$ (Fig. 3 C). Since K^+ is a competitor, one would intuitively expect the CTX-binding rate in high K^+ to be at most equal to that in high Na^+, but not greater. Nevertheless, this counterintuitive result has precedents. The CTX-R25Q variant binds Shaker two to three times faster in high external K^+ than in Na^+ Additionally, at 20 mM ionic strength, CTX exhibits a fourfold higher association rate in K^+ compared with Na^+ solutions (Moldenhauer et al., 2019). Similarly, across a wide range of ionic concentrations, CTX binds BK channels approximately twofold faster in K^+ versus Na^+ (Anderson et al., 1988). These observations point to a complex binding mechanism—potentially consistent with Scheme 2.

In this framework, the conceptual separation between the initial binding event and the formation of the fully bound complex could help explain the anomaly. We may speculate that while the absolute collision frequency (k_1) remains similar under both ionic conditions, the fraction of effective collisions—given by $k_2/(k_{-1} + k_2)$, remains constant in high Na^+ but increases with temperature in high K^+. Thus, CTX and K^+ may not directly compete for binding the channel. Instead, once CTX is bound, its Lys27 amino group competes with K^+ for occupancy of the S1 site. This leads to a configurational search phase that ends when S1 becomes available and Lys27 locks in. All steps in this exploration are accelerated at higher temperatures, shortening the lifetime of the intermediate *Ch*Tx*. At 20°C, this intermediate is sufficiently long-lived to equalize the association rates in *Hi-K*$^+$ and *Hi-Na*$^+$ conditions.

Association rate and wobbling?

The structure of the CTX/Kv 1.2/2.1 complex crystallized in Cs^+ salt may provide a physical picture of some early stage of wobbling (PDB ID 4JTC; [Banerjee et al., 2013]). Unlike the CTX–Kv1.2/2.1 structure obtained in K^+ salts, where S1 is devoid of K^+ electron density (Fig. 6 A), the complex crystallized in Cs^+ shows a Cs^+ ion occupying S1, while the amino group of Lys27 is retracted ∼2–3-Å back into the CTX body (Fig. 6 B; [Banerjee et al., 2013]). This crystal structure captures a permeant ion residing in S1 while the ε-amino group of Lys27 is displaced. This conformation aligns with MD simulation snapshots of the VGKC–CTX complex in K^+, taken ∼10 ns after applying a 500-mV

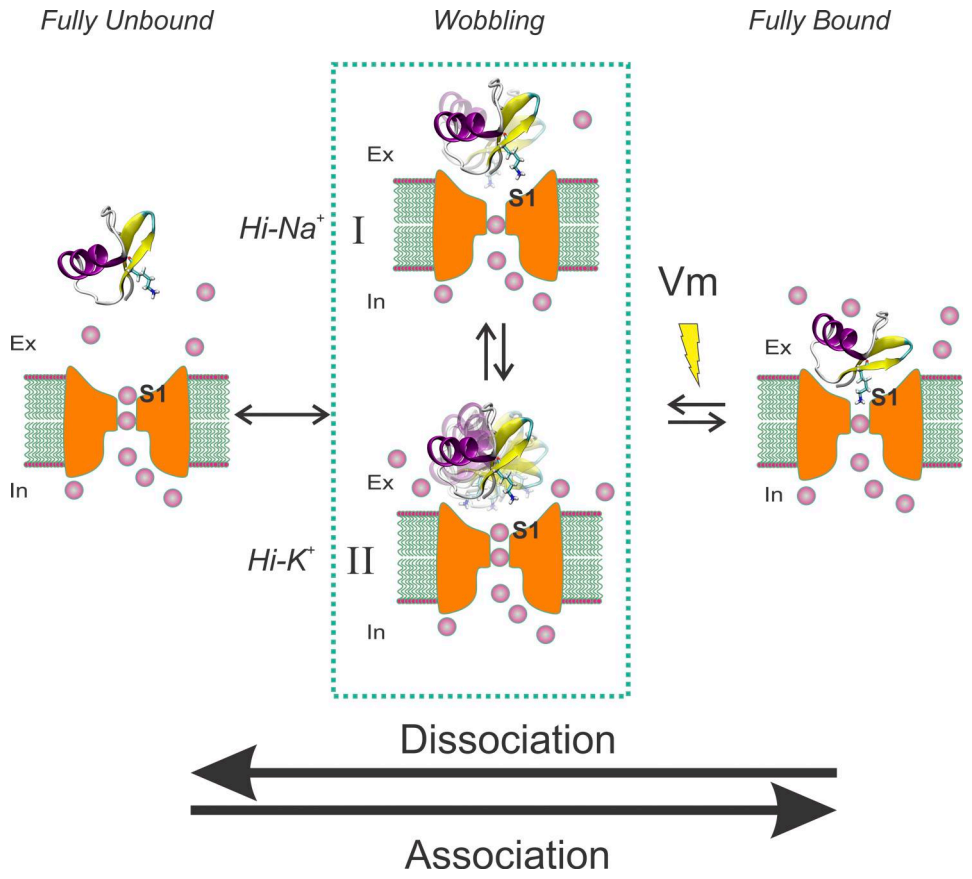

Figure 7. **Wobbling intermediates the dissociation and association pathways.** Association: The freely diffusing toxin binds partially and wobbles until the Lys27 ε-amino group binds into S1 to get fully bound. Dissociation: The fully bound toxin begins wobbling when, enhanced by the transmembrane voltage, the Lys27 amino group detaches from S1 (Wobbling I). While S1 remains empty, the Lys27 ε-amino group may return, or it can be occupied by another K^+, delaying fully bound conformation (Wobbling II). Wobbling I is favored in high external Na^+, while Wobbling II is favored in high external K^+.

transmembrane electric field (Fig. 6 C; Moldenhauer et al. [2019]: data available at https://doi.org/10.5061/dryad.0p77qk4). As in the Cs^+ crystal, Fig. 6, C and D, shows the amino group of the Lys27 side chain retracted >3-Å above S1, which is occupied by a K^+ ion. This represents the early stage of wobbling, as later in the simulation, the ε-amino group of Lys27 can be found up to 10-Å above its native position (Moldenhauer et al., 2019).

The dynamic behavior of the intermediate complex may resemble what we previously described as wobbling (Moldenhauer et al., 2019). High external potassium concentrations would significantly increase the occupancy of S1, thereby slowing k_2, without affecting the effective collision rate, which remains diffusion controlled (Wobbling: II in Fig. 7). A potential reason for the extended lifetime of the *Ch*Tx* intermediate complex could be that occupancy of S1 by the Lys27 side chain is antagonized by potassium ions. In contrast, under high external Na^+ conditions, S1 would remain unoccupied for a greater fraction of time. As a result, wobbling should be briefer and not rate limiting (Wobbling: I in Fig. 7), and thus would not contribute a significant enthalpic component. This separation between CTX binding and Lys27 clicking could explain the high association rate observed in high K^+. While CTX binding itself may not compete with K^+, the Lys27 clicking step does. Therefore, the detachment of the Lys27 amino group from S1, the most distinctive feature of wobbling, may be a shared characteristic of the *Ch*Tx* intermediate complex.

A two-way street for the reaction coordinates

Does wobbling represent the transition state in the CTX-binding reaction pathway? We propose that the specific energetic impact of external K^+ on toxin binding and unbinding kinetics results from K^+ competitively preventing the Lys27 ε-amino group from occupying S1 while the toxin is wobbling (Wobbling in Fig. 7). A similar wobbling pattern (I and II) may occur in both directions of the reaction coordinate. In the association pathway, Shaker and CTX form a binding intermediate that explores geometrical complementarity, establishing a series of transient interactions along the reaction trajectory until the Lys27 ε-amino group, competing with external K^+, clicks into S1 to form the fully bound state. This pathway could account for the larger activation enthalpy and entropy observed for k_{on} in *Hi-K*$^+$ compared with *Hi-Na*$^+$. As expected for an energy-conservative process, the reverse pathway would be traversed during dissociation (Dill and Bromberg, 2011).

The wobbling behavior of CTX in Shaker K channels permits access to the selectivity filter from the extracellular when the channel is blocked by CTX, favoring permeant ions over non-

permeant ones (Moldenhauer et al., 2019). Here, we further propose that wobbling contributes to the increased association and dissociation enthalpies when K^+ is the main external cation, suggesting that wobbling is briefer and not rate limiting when the external ion is non-permeant. Thus, it remains to be tested whether a relationship exists between ion-binding enthalpy of CTX binding and permeation.

Wobbling can be economically described by a two-step binding mechanism in which a positively charged neurotoxin binds to an oppositely charged molecular receptor, as outlined in Scheme 2. This mechanism may be shared by other neurotoxins that act on the external vestibule of K^+ channels, such as κ-PVIIA from *Conus*, *ShK* from sea anemone, and dendrotoxin from mamba (Kalman et al., 1998; García et al., 1999; Imredy and MacKinnon, 2000). Wobbling has been suggested for κ-PVIIA, as its dissociation rate from the open channel is insensitive to ionic strength, whereas in the closed channel it is highly dependent on it. This observation suggests that in the open channel, ionic strength is buffered by the intracellular environment via the pore, while in closed channels that connection is disrupted by the internal gate (Naranjo and Díaz-Franulic, 2020). Evolution may have favored a binding mechanism that incorporates wobbling because it relaxes the orientation constraints required for productive encounters, thereby increasing the overall fraction of effective collisions. Targeting VGKCs, alongside other neurotoxins in scorpion venom, contributes to a rapid excitotoxic effect that immobilizes the prey (Terlau et al., 1996).

Data availability

The data underlying all figures are available in the online supplemental material.

Acknowledgments

Christopher J. Lingle served as editor.

We thank Drs. Ignacio Díaz-Franulic and Antonio Peña for their careful reading and insightful discussions.

This work was funded by Fondo Nacional de Desarrollo Científico y Tecnológico (FONDECYT) 1211366 (to D. Naranjo) and FONDECYT 1211143 (to H. Poblete). F. Salas-Sepulveda acknowledges the Doctoral fellowship ANID-21241753. We are sincerely thankful to the editors and reviewers for their careful and constructive support throughout the process.

Author contributions: N. Navarro-Quezada: formal analysis, investigation, and resources. F. Salas-Sepulveda: formal analysis, investigation, methodology, validation, visualization, and writing—review and editing. H. Poblete: conceptualization, data curation, formal analysis, funding acquisition, investigation, methodology, project administration, resources, software, supervision, validation, visualization, and writing—original draft, review, and editing. D. Naranjo: conceptualization, data curation, formal analysis, funding acquisition, investigation, methodology, project administration, resources, supervision, validation, visualization, and writing—original draft, review, and editing.

Disclosures: The authors declare no competing interests exist.

Submitted: 12 April 2024
Revised: 7 February 2025
Revised: 1 June 2025
Accepted: 1 July 2025

References

Aggarwal, S.K., and R. MacKinnon. 1996. Contribution of the S4 segment to gating charge in the Shaker K^+ channel. *Neuron*. 16:1169–1177. https://doi.org/10.1016/s0896-6273(00)80143-9

Anderson, C.S., R. MacKinnon, C. Smith, and C. Miller. 1988. Charybdotoxin block of single Ca^{2+}-activated K^+ channels. Effects of channel gating, voltage, and ionic strength. *J. Gen. Physiol.* 91:317–333. https://doi.org/10.1085/jgp.91.3.317

Aqvist, J., and V. Luzhkov. 2000. Ion permeation mechanism of the potassium channel. *Nature*. 404:881–884. https://doi.org/10.1038/35009114

Banerjee, A., A. Lee, E. Campbell, and R. Mackinnon. 2013. Structure of a pore-blocking toxin in complex with a eukaryotic voltage-dependent K(+) channel. *Elife*. 2:e00594. https://doi.org/10.7554/eLife.00594

Bernèche, S., and B. Roux. 2001. Energetics of ion conduction through the K^+ channel. *Nature*. 414:73–77. https://doi.org/10.1038/35102067

Castaneda-Agullo, M., L.M. Del Castillo, J.R. Whitaker, and A.L. Tappel. 1961. Effect of ionic strength on the kinetics of trypsin and alpha chymotrypsin. *J. Gen. Physiol.* 44:1103–1120. https://doi.org/10.1085/jgp.44.6.1103

Díaz-Franulic, I., V. González-Pérez, H. Moldenhauer, N. Navarro-Quezada, and D. Naranjo. 2018. Gating-induced large aqueous volumetric remodeling and aspartate tolerance in the voltage sensor domain of Shaker K(+) channels. *Proc. Natl. Acad. Sci. USA*. 115:8203–8208. https://doi.org/10.1073/pnas.1806578115

Díaz-Franulic, I., R.V. Sepúlveda, N. Navarro-Quezada, F. González-Nilo, and D. Naranjo. 2015. Pore dimensions and the role of occupancy in unitary conductance of Shaker K channels. *J. Gen. Physiol.* 146:133–146. https://doi.org/10.1085/jgp.201411353

Dill, K., and S. Bromberg. 2011. Molecular Driving Forces: Statistical Thermodynamics In Biology, Chemistry, Physics, and Nanoscience. Taylor & Francis Group, New York.

Escobar, L., M.J. Root, and R. MacKinnon. 1993. Influence of protein surface charge on the bimolecular kinetics of a potassium channel peptide inhibitor. *Biochemistry*. 32:6982–6987. https://doi.org/10.1021/bi00078a024

French, R.J., E. Prusak-Sochaczewski, G.W. Zamponi, S. Becker, A.S. Kularatna, and R. Horn. 1996. Interactions between a pore-blocking peptide and the voltage sensor of the sodium channel: An electrostatic approach to channel geometry. *Neuron*. 16:407–413. https://doi.org/10.1016/s0896-6273(00)80058-6

Frisch, C., A.R. Fersht, and G. Schreiber. 2001. Experimental assignment of the structure of the transition state for the association of barnase and barstar. *J. Mol. Biol.* 308:69–77. https://doi.org/10.1006/jmbi.2001.4577

García, E., M. Scanlon, and D. Naranjo. 1999. A marine snail neurotoxin shares with scorpion toxins a convergent mechanism of blockade on the pore of voltage-gated K channels. *J. Gen. Physiol.* 114:141–157. https://doi.org/10.1085/jgp.114.1.141

Goldstein, S.A., and C. Miller. 1992. A point mutation in a Shaker K^+ channel changes its charybdotoxin binding site from low to high affinity. *Biophys. J.* 62:5–7. https://doi.org/10.1016/S0006-3495(92)81760-5

Goldstein, S.A., and C. Miller. 1993. Mechanism of charybdotoxin block of a voltage-gated K^+ channel. *Biophys. J.* 65:1613–1619. https://doi.org/10.1016/S0006-3495(93)81200-1

González-Pérez, V., A. Neely, C. Tapia, G. González-Gutiérrez, G. Contreras, P. Orio, V. Lagos, G. Rojas, T. Estévez, K. Stack, and D. Naranjo. 2008. Slow inactivation in Shaker K channels is delayed by intracellular tetraethylammonium. *J. Gen. Physiol.* 132:633–650. https://doi.org/10.1085/jgp.200810057

Gross, A., and R. MacKinnon. 1996. Agitoxin footprinting the shaker potassium channel pore. *Neuron*. 16:399–406. https://doi.org/10.1016/s0896-6273(00)80057-4

Harel, M., A. Spaar, and G. Schreiber. 2009. Fruitful and futile encounters along the association reaction between proteins. *Biophys. J.* 96:4237–4248. https://doi.org/10.1016/j.bpj.2009.02.054

Heginbotham, L., and R. MacKinnon. 1993. Conduction properties of the cloned Shaker K^+ channel. *Biophys. J.* 65:2089–2096. https://doi.org/10.1016/S0006-3495(93)81244-X

Hristova, K., and W.C. Wimley. 2023. Determining the statistical significance of the difference between arbitrary curves: A spreadsheet method. *PLoS One*. 18:e0289619. https://doi.org/10.1371/journal.pone.0289619

Imredy, J.P., and R. MacKinnon. 2000. Energetic and structural interactions between delta-dendrotoxin and a voltage-gated potassium channel. *J. Mol. Biol.* 296:1283–1294. https://doi.org/10.1006/jmbi.2000.3522

Kahler, U., A.S. Kamenik, F. Waibl, J. Kraml, and K.R. Liedl. 2020. Protein-protein binding as a two-step mechanism: Preselection of encounter poses during the binding of BPTI and trypsin. *Biophys. J.* 119:652–666. https://doi.org/10.1016/j.bpj.2020.06.032

Kalman, K., M.W. Pennington, M.D. Lanigan, A. Nguyen, H. Rauer, V. Mahnir, K. Paschetto, W.R. Kem, S. Grissmer, G.A. Gutman, et al. 1998. ShK-Dap22, a potent Kv1.3-specific immunosuppressive polypeptide. *J. Biol. Chem.* 273:32697–32707. https://doi.org/10.1074/jbc.273.49.32697

LeMasurier, M., L. Heginbotham, and C. Miller. 2001. KcsA: it's a potassium channel. *J. Gen. Physiol.* 118:303–314. https://doi.org/10.1085/jgp.118.3.303

Long, S.B., E.B. Campbell, and R. Mackinnon. 2005. Crystal structure of a mammalian voltage-dependent Shaker family K^+ channel. *Science*. 309:897–903. https://doi.org/10.1126/science.1116269

MacKinnon, R. 1991. Determination of the subunit stoichiometry of a voltage-activated potassium channel. *Nature*. 350:232–235. https://doi.org/10.1038/350232a0

MacKinnon, R., and C. Miller. 1988. Mechanism of charybdotoxin block of the high-conductance, Ca^{2+}-activated K^+ channel. *J. Gen. Physiol.* 91:335–349. https://doi.org/10.1085/jgp.91.3.335

Meyer, R., and S.H. Heinemann. 1997. Temperature and pressure dependence of Shaker K^+ channel N- and C-type inactivation. *Eur. Biophys. J.* 26:433–445. https://doi.org/10.1007/s002490050098

Miller, C. 1990. Diffusion-controlled binding of a peptide neurotoxin to its K^+ channel receptor. *Biochemistry*. 29:5320–5325. https://doi.org/10.1021/bi00474a016

Moldenhauer, H., I. Díaz-Franulic, F. González-Nilo, and D. Naranjo. 2016. Effective pore size and radius of capture for K(+) ions in K-channels. *Sci. Rep.* 6:19893. https://doi.org/10.1038/srep19893

Moldenhauer, H., I. Díaz-Franulic, H. Poblete, and D. Naranjo. 2019. Trans-toxin ion-sensitivity of charybdotoxin-blocked potassium-channels reveals unbinding transitional states. *Elife*. 8:e46170. https://doi.org/10.7554/eLife.46170

Moscoso, C., A. Vergara-Jaque, V. Márquez-Miranda, R.V. Sepulveda, I. Valencia, I. Díaz-Franulic, F. González-Nilo, and D. Naranjo. 2012. K(+) conduction and Mg(2)(+) blockade in a shaker Kv-channel single point mutant with an unusually high conductance. *Biophys. J.* 103:1198–1207. https://doi.org/10.1016/j.bpj.2012.08.015

Naranjo, D. 2002. Inhibition of single Shaker K channels by kappa-conotoxin-PVIIA. *Biophys. J.* 82:3003–3011. https://doi.org/10.1016/S0006-3495(02)75641-5

Naranjo, D., and I. Díaz-Franulic. 2020. Binding of kappa-conotoxin-PVIIA to open and closed shaker K-channels are differentially affected by the ionic strength. *Mar. Drugs*. 18:533. https://doi.org/10.3390/md18110533

Naranjo, D., H. Moldenhauer, M. Pincuntureo, and I. Díaz-Franulic. 2016. Pore size matters for potassium channel conductance. *J. Gen. Physiol.* 148:277–291. https://doi.org/10.1085/jgp.201611625

Neyton, J., and C. Miller. 1988. Discrete Ba2+ block as a probe of ion occupancy and pore structure in the high-conductance Ca^{2+} -activated K^+ channel. *J. Gen. Physiol.* 92:569–586. https://doi.org/10.1085/jgp.92.5.569

Oliva, C., V. González, and D. Naranjo. 2005. Slow inactivation in voltage gated potassium channels is insensitive to the binding of pore occluding peptide toxins. *Biophys. J.* 89:1009–1019. https://doi.org/10.1529/biophysj.105.060152

Ranganathan, R., J.H. Lewis, and R. MacKinnon. 1996. Spatial localization of the K^+ channel selectivity filter by mutant cycle-based structure analysis. *Neuron*. 16:131–139. https://doi.org/10.1016/s0896-6273(00)80030-6

Scanlon, M.J., D. Naranjo, L. Thomas, P.F. Alewood, R.J. Lewis, and D.J. Craik. 1997. Solution structure and proposed binding mechanism of a novel potassium channel toxin kappa-conotoxin PVIIA. *Structure*. 5:1585–1597. https://doi.org/10.1016/s0969-2126(97)00307-9

Schreiber, G., and A.R. Fersht. 1995. Energetics of protein-protein interactions: Analysis of the barnase-barstar interface by single mutations and double mutant cycles. *J. Mol. Biol.* 248:478–486. https://doi.org/10.1016/s0022-2836(95)80064-6

Schreiber, G., G. Haran, and H.-X. Zhou. 2009. Fundamental aspects of protein-protein association kinetics. *Chem. Rev.* 109:839–860. https://doi.org/10.1021/cr800373w

Selvakumar, P., A.I. Fernández-Mariño, N. Khanra, C. He, A.J. Paquette, B. Wang, R. Huang, V.V. Smider, W.J. Rice, K.J. Swartz, and J.R. Meyerson. 2022. Structures of the T cell potassium channel Kv1.3 with immunoglobulin modulators. *Nat. Commun.* 13:3854. https://doi.org/10.1038/s41467-022-31285-5

Stocker, M., and C. Miller. 1994. Electrostatic distance geometry in a K^+ channel vestibule. *Proc. Natl. Acad. Sci. USA*. 91:9509–9513. https://doi.org/10.1073/pnas.91.20.9509

Terlau, H., A. Boccaccio, B.M. Olivera, and F. Conti. 1999. The block of Shaker K+ channels by kappa-conotoxin PVIIA is state dependent. *J. Gen. Physiol.* 114:125–140. https://doi.org/10.1085/jgp.114.1.125

Terlau, H., K.J. Shon, M. Grilley, M. Stocker, W. Stühmer, and B.M. Olivera. 1996. Strategy for rapid immobilization of prey by a fish-hunting marine snail. *Nature*. 381:148–151. https://doi.org/10.1038/381148a0

Volkov, A.N., J.A.R. Worrall, E. Holtzmann, and M. Ubbink. 2006. Solution structure and dynamics of the complex between cytochrome *c* and cytochrome *c* peroxidase determined by paramagnetic NMR. *Proc. Natl. Acad. Sci. USA*. 103:18945–18950. https://doi.org/10.1073/pnas.0603551103

Supplemental material

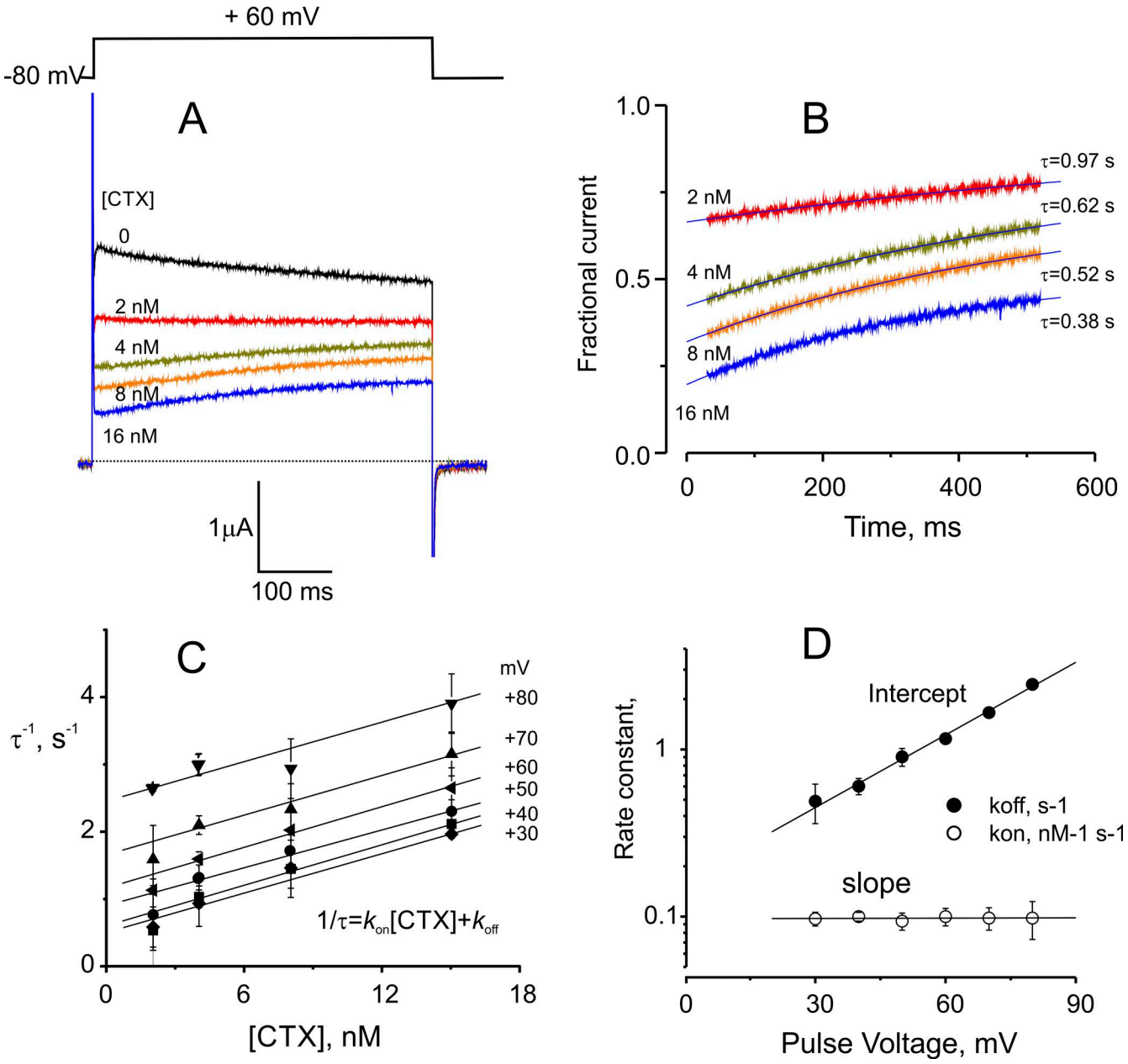

Figure S1. **Relaxation rates as function of CTX concentration. (A)** Family of TEVC traces recorded at +60 mV from the same oocyte in the absence and presence of increasing CTX concentrations in the bath. These measurements were carried out in *Hi-Na*$^+$ solution. **(B)** Point-by-point current ratios between the traces at different CTX concentrations, divided by the control trace (black), as described in Materials and methods. The trace colors match the CTX concentrations indicated in A. The blue line on top of each trace is a single-exponential fit to the relaxation, and the corresponding τ values are shown to the right of each trace. **(C)** Plot of 1/τ versus [CTX] for several oocytes and voltage pulses applied at different potentials. The continuous lines are linear fits, where the slope corresponds to k_{on} and the intercept to k_{off}. Each measurement is the average ± SD for three to five experiments. **(D)** Linear fit parameters from the data in C, plotted as a function of voltage. The solid lines are fits of Eq. 4 with the following parameters: k_{ono} = 0.045 ± 0.02 nM^{-1} s^{-1}, zδ = 0.15 ± 0.09 and k_{offo} = 0.21 ± 0.052 s^{-1}, zδ = 0.78 ± 0.09. Error bars represent the SEM. See also Data S1 for underlying data.

Provided online are Data S1, Data S2, Data S3, Data S4, Data S5, and Data S6. Data S1 contains the original data for the Fig. S1; Data S1 contains the original data for Fig. 1; Data S2 contains the original data for Fig. 2; Data S3 contains the original experimental traces

used for Fig. 2; Data S4 contains a summary of experimental data in open channels for Figs. 3 and 5; Data S5 and Data S6 contain the data for Figs. 4 and 5.